

Validity of extracting photoionization time delay from the first moment of streaking spectrogram

Chang-Li Wei(魏长立), Xi Zhao(赵曦)

Citation: Chin. Phys. B . 2019, 28(1): 013201. **doi:** 10.1088/1674-1056/28/1/013201
Journal homepage: http://cpb.iphy.ac.cn; http://iopscience.iop.org/cpb

What follows is a list of articles you may be interested in

Low-order harmonic generation of hydrogen molecular ion in laser field studied by the two-state model

Ling-Ling Du(杜玲玲), Guo-Li Wang(王国利), Peng-Cheng Li(李鹏程), Xiao-Xin Zhou(周效信)

Chin. Phys. B . 2018, 27(11): 113201. **doi:** 10.1088/1674-1056/27/11/113201

Backward rescattered photoelectron holography in strong-field ionization

Fujun Chen(陈富军), Ruxian Yao(姚汝贤), Jianghua Luo(罗江华), Changqing Wang(王长清)

Chin. Phys. B . 2018, 27(10): 103202. **doi:** 10.1088/1674-1056/27/10/103202

Numerical tests of theoretical models describing ionization of H(1s) atom by linearly polarized flat pulse of laser radiation

Jarosław H Bauer, Min Deng(邓敏)

Chin. Phys. B . 2018, 27(9): 093202. **doi:** 10.1088/1674-1056/27/9/093202

Effect of elliptical polarizations on nonsequential double ionization in two-color elliptically polarized laser fields

Tong-Tong Xu(徐彤彤), Jia-He Chen(陈佳贺), Xue-Fei Pan(潘雪飞), Hong-Dan Zhang(张宏丹), Shuai Ben(贲帅), Xue-Shen Liu(刘学深)

Chin. Phys. B . 2018, 27(9): 093201. **doi:** 10.1088/1674-1056/27/9/093201

Method of accurately calculating mean field operator in multi-configuration time-dependent Hartree-Fock frame

Li Wen-Liang, Zhang Ji, Yao Hong-Bin

Chin. Phys. B . 2013, 22(9): 093202. **doi:** 10.1088/1674-1056/22/9/093202

Validity of extracting photoionization time delay from the first moment of streaking spectrogram*

Chang-Li Wei(魏长立)[1] and Xi Zhao(赵曦)[2,†]

[1] School of Physics and Electronics, Qiannan Normal College for Nationalities, Duyun 558000, China
[2] Department of Physics, Kansas State University, Manhattan, KS 66506, USA

(Received 12 September 2018; revised manuscript received 26 October 2018; published online 27 December 2018)

Photoionization time delays have been studied in many streaking experiments in which an attosecond pulse is used to ionize the atomic or solid state target in the presence of a dressing infrared laser field. Among the methods of extracting the time delay from the streaking spectrogram, the simplest one is to calculate the first moment of the spectrogram and to measure its offset relative to the vector potential of the infrared field. The first moment method has been used in many theoretical simulations and analysis of experimental data, but the meaning of this offset needs to be investigated. We simulate the spectrograms and compare the extracted time delay from the first moment with the input Wigner delay. In this study, we show that the first moment method is valid only when the group delay dispersions corresponding to both the spectral phase of the attosecond pulse and the phase of the single-photon transition dipole matrix element of the target are small. Under such circumstance, the electron wave packet behaves like a classical particle and the extracted time delay can be related to a group delay in the photoionization process. To avoid ambiguity and confusion, we also suggest that the photoionization time delay be replaced by photoionization group delay and the Wigner time delay be replaced by Wigner group delay.

Keywords: photoionization time delay, strong laser field, attosecond science, first moment

PACS: 32.80.Rm, 42.50.Hz, 42.65.Ky **DOI:** 10.1088/1674-1056/28/1/013201

1. Introduction

With the advent of attosecond pulse trains (APT)[1] and isolated attosecond pulses (IAP)[2–4] since 2001, attosecond pulses have been used to initiate photoionization of atoms,[5–21] molecules,[22–26] and condensed materials.[27–32] The goal is that the attosecond electron wave packets generated can then be probed by another attosecond pulse with different time delays, therefore electron dynamics can be probed at attosecond timescale. This has not been possible so far, thus the "probe" is usually a moderately intense infrared laser. By measuring the continuum photoelectron spectra versus the time delay between the extreme ultraviolet (XUV) attosecond pulse and the infrared (IR) pulse, the two-dimensional photoelectron spectrogram can be obtained. Such an experimental setup is called attosecond streaking.[33] In fact, the streaking spectrogram is widely used to characterize attosecond pulses, by employing the "reconstruction of attosecond beating by interference of two-photon transition" (RABITT)[34] method for the characterization of APTs, and the "frequency-resolved optical gating for complete reconstruction of attosecond bursts" (FROG-CRAB) method[35] for the characterization of IAPs. To use RABITT or FROG-CRAB for attosecond pulse characterization, one has to know the photoionization transition dipole moment of the target. If the target is a rare gas atom, then the magnitude of the transition dipole as a function of the photoelectron energy is well known from the synchrotron radiation measurement; however, the phase of the transition dipole has to rely on theoretical calculations. On the other hand, if the fields of the attosecond pulse and the IR are known well, from the streaking spectrogram one would hope that the phase of the transition dipole can be retrieved.

Photoionization time delay has been a very controversial and widely debated topic in recent years (see the reviews[36,37]). To many people, this time delay means the delayed arrival of a photoelectron with respect to an imaginary reference particle at an imaginary detector. Clearly, such an imaginary delay is not directly measurable in the laboratory. It has to be derived under some theoretical model. It has been defined as the energy derivative of the phase of the photoelectron wave packet after a photoionization process. The modulus square of this wave packet is the well-known photoelectron signal that has been routinely measured in the laboratory over the years, but the determination of the phase has been elusive. With the availability of APT (or IAP), by perform-

*Project supported by the Talent Introduction Foundation of Qiannan Normal University of Nationalities, China (Grant No. qnsyrc201619), Natural Science Foundation of Guizhou Provincial Education Department for Young Talents, China (Grant No. Qian Education Contract KY[2017]339), and Chemical Sciences, Geosciences and Biosciences Division, Office of Basic Energy Sciences, Office of Science, U.S. Department of Energy (Grant No. DE-FG02-86ER13491).

†Corresponding author. E-mail: zhaoxi719@ksu.edu

© 2019 Chinese Physical Society and IOP Publishing Ltd

ing photoionization experiments in the presence of a moderately intense IR field, the phase difference (or the derivative of phase with respect to energy) of the photoelectron wave packet can be retrieved from the streaking spectrogram using the RABITT method[9–13] (or the FROG-CRAB method[16–18]). In the meanwhile, lots of theoretical studies have then been invoked to interpret the experimental observations.[37–48] One of the goals of these studies is to demonstrate that the streaking spectrogram would allow the extraction of photoionization time delay which in turn can be directly compared to the Wigner time delay.[49,50] The latter is defined as the energy derivative of the phase of the photoionization dipole transition matrix element.

Phase retrieval methods like the RABITT and the FROG-CRAB formally allow the extraction of the full phase difference or the full group delay. However, the procedure is rather tedious. Thus for years, photoionization time delays were obtained using the so-called first moment method in both experimental reports[27–30] and theoretical investigations.[41–47] In this method, one calculates the first moment of the spectrogram, compares it with the vector potential of the IR field, and then extracts a time delay which is the offset between the first moment and the vector potential. In this article, we simulate streaking spectrograms using various pulse parameters and atomic targets, and then compare the time delays extracted via the first moment method to the input Wigner delays. According to our investigation, the first moment method is in general inaccurate unless the group delay dispersions corresponding to the phase of both the attosecond pulse and the transition dipole are negligible.

This article is organized as follows. In Section 2, we briefly introduce some theoretical aspects of this work; we first give the mathematical description of the XUV pulse in Section 2.1, followed by the photoelectron wave packet and the single-photon transition dipole in Section 2.2; Section 2.3 introduces the strong field approximation (SFA) model for XUV–IR streaking and Section 2.4 introduces the first moment method to measure the photoionization time delay from streaking spectrograms. Section 3 shows our simulation results; in Section 3.1, we generate spectrograms based on the SFA model using various targets and XUV pulses to check the accuracy of the first moment method, while in Section 3.2, the spectrograms for Ne and Ar are generated by solving the time-dependent Schrödinger equation (TDSE) numerically in order to include the effect of the Coulomb field. We conclude this article in Section 4. Atomic units (a.u.) are used unless otherwise stated.

2. Theoretical background of photoionization time delay

2.1. Description of the XUV pulse

Consider an atom ionized by a weak XUV pulse whose electric field is linearly polarized along the z-axis. The electric field strength in time domain takes the form

$$E_{\mathrm{XUV}}(t) = \sqrt{I(t)}\cos[\Omega_0 t + \zeta(t)], \tag{1}$$

where Ω_0 is its central frequency, $I(t)$ is the temporal intensity envelope, and $\zeta(t)$ is the temporal phase. One can take the Fourier transform to get the spectrum in frequency domain

$$\tilde{E}_{\mathrm{XUV}}(\Omega) = U(\Omega)\,\mathrm{e}^{\mathrm{i}\Phi(\Omega)} = \int_{-\infty}^{+\infty} E_{\mathrm{XUV}}(t)\,\mathrm{e}^{\mathrm{i}\Omega t}\,\mathrm{d}t. \tag{2}$$

Here, $U(\Omega)$ and $\Phi(\Omega)$ are the spectral amplitude and phase, respectively. From the phase $\Phi(\Omega)$, we can define the XUV group delay

$$\tau^{\mathrm{XUV}}(\Omega) = \frac{\mathrm{d}}{\mathrm{d}\Omega}\Phi(\Omega), \tag{3}$$

and the group delay dispersion (GDD)

$$\mathrm{GDD}^{\mathrm{XUV}}(\Omega) = \frac{\mathrm{d}}{\mathrm{d}\Omega}\tau^{\mathrm{XUV}}(\Omega) = \frac{\mathrm{d}^2}{\mathrm{d}\Omega^2}\Phi(\Omega). \tag{4}$$

For a narrow-band pulse with central frequency Ω_0, the quantity $\tau_0^{\mathrm{XUV}} = \tau^{\mathrm{XUV}}(\Omega_0)$ describes an overall shift of the pulse envelope along the time axis, that is, the group delay, while $\mathrm{GDD}^{\mathrm{XUV}}(\Omega_0)$ is a measurement of the attochirp which affects the pulse duration and the temporal phase. To be more specific, assume the spectral amplitude takes the Gaussian form

$$U(\Omega) = U_0\,\mathrm{e}^{-2\ln 2\frac{(\Omega-\Omega_0)^2}{(\Delta\Omega)^2}}, \tag{5}$$

where the full width at half maximum (FWHM) bandwidth of the pulse is given by $\Delta\Omega$. If $\Phi(\Omega) = 0$, one can easily get the temporal envelope

$$I(t) = I_0\,\mathrm{e}^{-4\ln 2\frac{t^2}{(\Delta t)^2}}, \tag{6}$$

and the phase $\zeta(t) = 0$. Here, the FWHM duration Δt and the bandwidth $\Delta\Omega$ are related by

$$\Delta\Omega\Delta t = 4\ln 2. \tag{7}$$

The pulses with $\mathrm{GDD}^{\mathrm{XUV}}(\Omega) = 0$ are called transform-limited (TL), like in the case above. The TL pulse can also have a constant group delay $\tau^{\mathrm{XUV}}(\Omega) = \tau_0^{\mathrm{XUV}}$, $\Phi(\Omega) = \tau_0^{\mathrm{XUV}}(\Omega - \Omega_0)$. In the time domain, this results in a delayed pulse $I(t - \tau_0^{\mathrm{XUV}})$.

What we are more interested in is the effect of attochirp. Suppose the pulse has a linear chirp, $\mathrm{GDD}^{\mathrm{XUV}}(\Omega) = \mathrm{GDD}^{\mathrm{XUV}}$, $\tau^{\mathrm{XUV}}(\Omega) = \mathrm{GDD}^{\mathrm{XUV}}(\Omega - \Omega_0)$, and $\Phi(\Omega) = \frac{1}{2}\mathrm{GDD}^{\mathrm{XUV}}(\Omega - \Omega_0)^2$. The temporal envelope still takes the form of Eq. (6) but the FWHM duration Δt is now determined

by

$$\Delta\Omega\Delta t = 4\ln 2\sqrt{1+\xi^2}, \tag{8}$$

where $\xi = \mathrm{GDD}^{\mathrm{XUV}}\frac{(\Delta\Omega)^2}{4\ln 2}$ is another parameter to measure attochirp. Clearly, equation (8) shows that the pulse is stretched in the time domain due to attochirp. The temporal phase becomes quadratic

$$\zeta(t) = \frac{1}{2}\alpha t^2 - \frac{1}{2}\arctan\xi, \tag{9}$$

where the parameter $\alpha = \mathrm{GDD}^{\mathrm{XUV}}\frac{(\Delta\Omega)^2}{(\Delta t)^2}$.

2.2. Photoelectron wave packet and single-photon transition dipole

If the XUV pulse is weak (typically 10^{11} W/cm^2 in peak intensity), one can apply the first-order perturbation theory to evaluate the electron wave packet ionized from the target atom. In this article, we focus on the photoelectron emitted along the same direction as the electric field polarization (z-axis). In the frequency domain, the wave packet can be expressed as

$$\tilde{W}(\Omega) = d(E)\tilde{E}_{\mathrm{XUV}}(\Omega). \tag{10}$$

Here, Ω can be interpreted as the XUV photon energy. $E = \Omega - I_{\mathrm{p}}$ is the electron energy with I_{p} being the ionization potential energy. Equation (10) manifests that the wave packet $W(\Omega)$ is to some extent a replica of the XUV pulse, but also includes the modulation of the single-photon dipole transition matrix element $d(E) = \langle E\hat{z}|z|i\rangle$. The initial state is denoted by $|i\rangle$, while $|E\hat{z}\rangle$ is the continuum state in which the electron has an asymptotic momentum $p = \sqrt{2E}$ toward the $+z$ direction. The initial and final states are eigenstates of the field-free Hamiltonian of the target atom. Here, we normalize the continuum states by electron energy, that is, $\langle E\hat{z}|E'\hat{z}\rangle = \delta(E-E')$.

The transition dipole $d(E)$ can be calculated within the single-active-electron (SAE) approximation. One can expand the continuum wave function $|E\hat{z}\rangle$ into partial waves and then calculate the matrix element for different channels separated by angular momentum. The matrix element will depend on the phase shift of the related partial wave, including both the long-range Coulomb phase shift and the short-range phase shift. For example, considering the ionization from the outermost shell of Ne (2p shell) or Ar (3p shell), the dipole $d(E)$ can be given by[51]

$$d(E) = \sqrt{\frac{1}{12\pi}}\left\{\mathrm{e}^{\mathrm{i}[\sigma_0(E)+\delta_0(E)]}\langle u_{E0}|r|u_i\rangle - 2\,\mathrm{e}^{\mathrm{i}[\sigma_2(E)+\delta_2(E)]}\langle u_{E2}|r|u_i\rangle\right\}. \tag{11}$$

Here, $u_{EL}(r)$ and $u_i(r)$ are the radial wave functions for the bound and continuum electron, σ_L is the Coulomb phase shift, and δ_L is the short-range phase shift. Details of evaluating the transition dipole can be found in Ref. [51]. For a many-electron atom, electron correlation may need to be taken into account; therefore, the expression of the transition dipole may become more complicated, especially when the so-called interchannel couplings are included. However, in general, one can always write the dipole matrix element for the transition from an initial state to a well-defined continuum electronic state in the $+z$ direction by its amplitude and phase: $d(E) = |d(E)|\,\mathrm{e}^{\mathrm{i}\eta(E)}$. The dipole phase $\eta(E)$ plays a critical role in the study of photoionization time delay.

From Eq. (10), we know the phase of the electron wave packet depends not only on the XUV phase $\Phi(\Omega)$ but also on the dipole phase $\eta(E)$. Similar to the above discussions for XUV pulses, one can introduce group delay and GDD for the dipole phase as follows:

$$\tau^{\mathrm{dip}}(E) = \frac{\mathrm{d}}{\mathrm{d}E}\eta(E), \tag{12}$$

$$\mathrm{GDD}^{\mathrm{dip}}(E) = \frac{\mathrm{d}}{\mathrm{d}E}\tau^{\mathrm{dip}}(E) = \frac{\mathrm{d}^2}{\mathrm{d}E^2}\eta(E). \tag{13}$$

The group delay τ^{dip} is often referred to as Wigner delay. The original Wigner delay was introduced for short-range scattering for a given partial wave.[49,50] Here, the concept of Wigner delay has been extended to photoionization as a half-scattering problem and to continuum electrons emitted toward a given direction. Moreover, the long-range Coulomb phase shift has been included in the expression of Wigner delay, as shown in Eq. (11). If the atom is ionized by a narrow-band XUV pulse, a narrow-band electron wave packet $\tilde{W}(\Omega)$ can be formed with a central photon energy Ω_0. Following the discussion on group delay in Section 2.1, the Wigner group delay $\tau_0^{\mathrm{dip}} = \tau^{\mathrm{dip}}(E_0)$ at $E_0 = \Omega_0 - I_{\mathrm{p}}$ can be interpreted as a shift on the time axis between the peak of the XUV pulse and the peak of the electron wave packet, as if the electron were "delayed" by this amount of time after being ionized by the XUV. In a typical experiment, such a photoionization time delay is derived from the streaking spectrogram. It does not convey an idea that the motion of the electron is delayed directly. Moreover, in the case of large GDD, this picture will be destroyed, as we shall see in Section 3.

2.3. The SFA model for streaking spectrograms

If the atom is ionized by the XUV pulse only, the measured photoelectron yield is proportional to $|\tilde{W}(\Omega)|^2$, but the phase information is not available. Nonlinear processes are required in order to pull out the phase and thus the time delay. Up to date, a lot of time delay measurements have been carried out by employing the streaking technique,[33] where the XUV photoionization is dressed by a phase-locked IR field. We assume that the electric field of the IR is polarized along

the same axis as the XUV field (z-axis). The total electric field becomes $E_{\rm IR}(t)+E_{\rm XUV}(t-t_{\rm d})$, where $t_{\rm d}$ is the time delay between XUV and IR. A positive $t_{\rm d}$ means the XUV comes after the IR. We assume the IR field can be expressed by

$$E_{\rm IR}(t)=F_0\cos^2\left(\frac{\pi t}{T_{\rm IR}}\right)\cos(\omega t+\phi_{\rm CEP}), \tag{14}$$

with $-\frac{T_{\rm IR}}{2}\le t\le\frac{T_{\rm IR}}{2}$. Here, ω is the central frequency of the IR field. The envelope takes a cosine-squared form with $T_{\rm IR}$ being the total duration. The FWHM duration can be estimated as $T_{\rm IR}/2.747$. $\phi_{\rm CEP}$ is the carrier-envelope-phase (CEP). The IR vector potential is given by $A(t)=-\int_{-\infty}^{t}E_{\rm IR}(t')\,{\rm d}t'$. In this work, we choose $\phi_{\rm CEP}=\pi/2$ such that $t=0$ is the peak position of $|A(t)|$ and $A(\infty)=0$. By varying the XUV–IR delay $t_{\rm d}$, a two-dimensional spectrogram or trace $S(E,t_{\rm d})$ can be accumulated. For a given $t_{\rm d}$, $S(E,t_{\rm d})$ is a function of electron energy E which describes the photoelectron yield per unit energy.

A simple quantum mechanical model of streaking was derived based on the SFA[52]

$$S(E,t_{\rm d})=\left|\int_{-\infty}^{\infty}E_{\rm XUV}(t-t_{\rm d})d\left(\frac{[p+A(t)]^2}{2}\right)\times{\rm e}^{-{\rm i}\int_t^{\infty}\left[pA(t')+\frac{1}{2}A^2(t')\right]{\rm d}t'}{\rm e}^{{\rm i}(E+I_{\rm p})t}\,{\rm d}t\right|^2. \tag{15}$$

Here, $d(E)$ is the single-photon dipole transition matrix element introduced before. The SFA model in Eq. (15) includes two basic assumptions. The first one is that the continuum electron propagates only in the IR field, while the Coulomb interaction between this electron and its parent ion is small so that it can be ignored. This is valid for electrons with large kinetic energy. The second assumption is that only the photoionization due to the XUV pulse is considered, while the multi-photon ionization induced by the IR field is not included in this model.

Applying the concept of electron wave packet, equation (15) can be approximated by

$$(E,t_{\rm d})\approx\left|\int_{-\infty}^{\infty}W(t-t_{\rm d})\times{\rm e}^{-{\rm i}\int_t^{\infty}\left[pA(t')+\frac{1}{2}A^2(t')\right]{\rm d}t'}{\rm e}^{{\rm i}(E+I_{\rm p})t}\,{\rm d}t\right|^2, \tag{16}$$

where

$$W(t)=\frac{1}{2\pi}\int_{-\infty}^{\infty}\tilde{W}(\Omega){\rm e}^{-{\rm i}\Omega t}\,{\rm d}\Omega \tag{17}$$

is the wave packet expressed in the time domain. Note that although equation (16) seems to be separating the XUV ionization and the IR streaking processes, it is only an approximation of the SFA model in Eq. (15) rather than an exact theory. The derivation was given in Ref. [53], where $E_{\rm XUV}(t)$ was expressed in terms of $\tilde{E}_{\rm XUV}(\Omega)=\dfrac{\tilde{W}(\Omega)}{d(E)}$ and $[d(E)]^{-1}$ was expanded in a Taylor series, which eventually leads to Eq. (16). To get this equation, all derivatives of $A(t)$ should be neglected, which requires that the exponential factor ${\rm e}^{-{\rm i}\int_t^{\infty}\left[pA(t')+\frac{1}{2}A^2(t')\right]{\rm d}t'}$ oscillates as a function of t with a period much shorter than the optical cycle of the IR field.[53] Based on Eq. (16), the FROG-CRAB method[35] has been used to extract the dipole phase and photoionization time delay.[16–18] The accuracy and limitation of the FROG-CRAB method were discussed recently by Zhao *et al.*[51,54]

2.4. The first moment method and photoionization time delay

In this article, we focus on extracting temporal information from the first moment of the streaking spectrogram. This idea stems from treating the electron wave packet as a classical particle. If an electron is released at $t=t_{\rm r}$ with a momentum p_0, then moves in the IR field as a free electron, finally the detected momentum of this electron after the IR is turned off would be $p_0-A(t_{\rm r})$. Suppose the electron is ionized by the XUV pulse $E_{\rm XUV}(t-t_{\rm d})$, the released time can be approximated by $t_{\rm r}=t_{\rm d}+\tau_0^{\rm XUV}+\tau_0^{\rm dip}$, in which $\tau_0^{\rm XUV}$ and $\tau_0^{\rm dip}$ are the XUV group delay and the Wigner group delay, respectively, as discussed in Section 2.2. Therefore, the detected momentum as a function of $t_{\rm d}$ goes like $p(t_{\rm d})=p_0-A(t_{\rm d}+\tau_0^{\rm XUV}+\tau_0^{\rm dip})$. Moreover, beyond the SFA model, after considering the modification of the electron trajectory due to the Coulomb field of the ionic core, an additional term called Coulomb–laser coupling (CLC) delay has been identified.[37,41] The CLC delay $\tau^{\rm CLC}(E)$ is a function of photoelectron energy E and IR frequency ω, independent of the target and the IR intensity. By including the single CLC delay $\tau_0^{\rm CLC}=\tau^{\rm CLC}(E_0)$ for the wave packet, finally we obtain

$$\begin{aligned}p(t_{\rm d}) &= p_0-A(t_{\rm d}+\tau^{\rm s})\\ &= p_0-A(t_{\rm d}+\tau_0^{\rm XUV}+\tau_0^{\rm dip}+\tau_0^{\rm CLC}).\end{aligned} \tag{18}$$

The CLC delay has been obtained analytically.[37] It is more prominent for low-energy electrons than high-energy ones. For example, $\tau_0^{\rm CLC}=-9$ as at $E_0=60$ eV, $\tau_0^{\rm CLC}=-14.8$ as at $E_0=40$ eV, and $\tau_0^{\rm CLC}=-33.3$ as at $E_0=20$ eV.

Starting from the spectrogram $S(E,t_{\rm d})$, one can calculate the first moment of the energy distribution

$$\bar{E}(t_{\rm d})=\frac{\int ES(E,t_{\rm d})\,{\rm d}E}{\int S(E,t_{\rm d})\,{\rm d}E}. \tag{19}$$

The quantity $\bar{E}(t_{\rm d})$ is often called center of energy (COE). Similarly, one can calculate the first moment of the momen-

tum distribution

$$\bar{p}(t_{\rm d}) = \frac{\int pS'(p,t_{\rm d})\,{\rm d}p}{\int S'(p,t_{\rm d})\,{\rm d}p}. \tag{20}$$

Here, $\bar{p}(t_{\rm d})$ can be named by center of momentum (COM). Note that $S'(p,t_{\rm d})$ in Eq. (20) is the electron yield per unit momentum, therefore $S'(p,t_{\rm d}) = pS(E,t_{\rm d})$. The time delay $\tau^{\rm s}$ in Eq. (18) can be extracted by comparing the COE or COM to the vector potential $-A(t_{\rm d})$ of the IR field and measuring their relative shift. Since the CLC delay is already known, once the XUV group delay is characterized, one can obtain the Wigner delay $\tau_0^{\rm W}$ from the extracted $\tau^{\rm s}$. Practically, one may measure two spectrograms corresponding to two targets or two ionization channels under the same combined XUV and IR field. By extracting the shift between the two COEs or COMs from these two spectrograms, it may be possible to cancel the XUV group delay to retrieve the Wigner delay difference between these two targets or two channels at a fixed photon energy. In Section 3, we will investigate the accuracy of this first moment method by using known transition dipoles to simulate the spectrogram under various circumstances.

3. Simulation results

3.1. Time delays extracted from SFA simulations

3.1.1. Simulation parameters

To simplify our discussion, let us first neglect the effect of Coulomb–laser coupling, which means we use the SFA Eq. (15) to calculate the streaking spectrogram and treat it as the experimental result. In our simulation, the XUV spectral intensity $U^2(\Omega)$ has a Gaussian form with $\Omega_0 = 60$ eV and FWHM $\Delta\Omega = 9.2$ eV, as plotted in Fig. 1(a). The XUV phase is $\Phi(\Omega) = \frac{1}{2}{\rm GDD}^{\rm XUV}(\Omega-\Omega_0)^2$, which corresponds to a linearly chirped XUV pulse with a constant GDD. Figure 1(b) gives the spectral phase of two XUV pulses: a transform-limited pulse (${\rm GDD}^{\rm XUV} = 0$, $\Delta t = 197$ as) and a chirped pulse (${\rm GDD}^{\rm XUV} = 2.57\times10^4$ as^2, $\Delta t = 410$ as). Figure 1(c) shows their corresponding group delay $\tau^{\rm XUV}(\Omega)$. At the central frequency, $\tau_0^{\rm XUV} = \tau^{\rm XUV}(\Omega_0) = 0$, therefore the peak of XUV envelope is always at $t = 0$. The IR field is 800 nm in wavelength, 6.6 fs in FWHM duration, and 10^{13} W/cm^2 in peak intensity. The profiles of $E_{\rm IR}(t)$ and $-A(t)$ are plotted in Fig. 1(d). The CEP is chosen to be $\pi/2$ so that the maximum of $-A(t)$ appears at $t = 0$.

Figure 2(a) gives the phase of transition dipoles $\eta(\Omega)$ that have been used in our simulation, as a function of the photon energy $\Omega = E + I_{\rm p}$. Four artificial targets (A–D) are used with $d(\Omega) = {\rm e}^{{\rm i}\eta(\Omega)}$ and $I_{\rm p} = 20$ eV. The transition dipole of Ne is also computed using a one-electron model potential.[55] The dipole phase of Ne is plotted in Fig. 2(a), in which this phase has been shifted vertically by a constant to satisfy $\eta(\Omega_0) = 0$ for better comparison with other targets. The Wigner delay $\tau^{\rm dip}(\Omega)$ and the delay dispersion ${\rm GDD}^{\rm dip}(\Omega)$ are given in Figs. 2(b) and 2(c), respectively. Target A has a constant Wigner delay $\tau^{\rm dip}(\Omega) = -40$ as. The Wigner delay of Ne changes slightly from 8 as to 5 as over the frequency region of the XUV pulse. However, the Wigner delay for targets B–D varies over the XUV bandwidth. The ${\rm GDD}^{\rm dip}(\Omega)$ increases linearly for target B while it is constant for target C (-658 as^2) and D (1975 as^2).

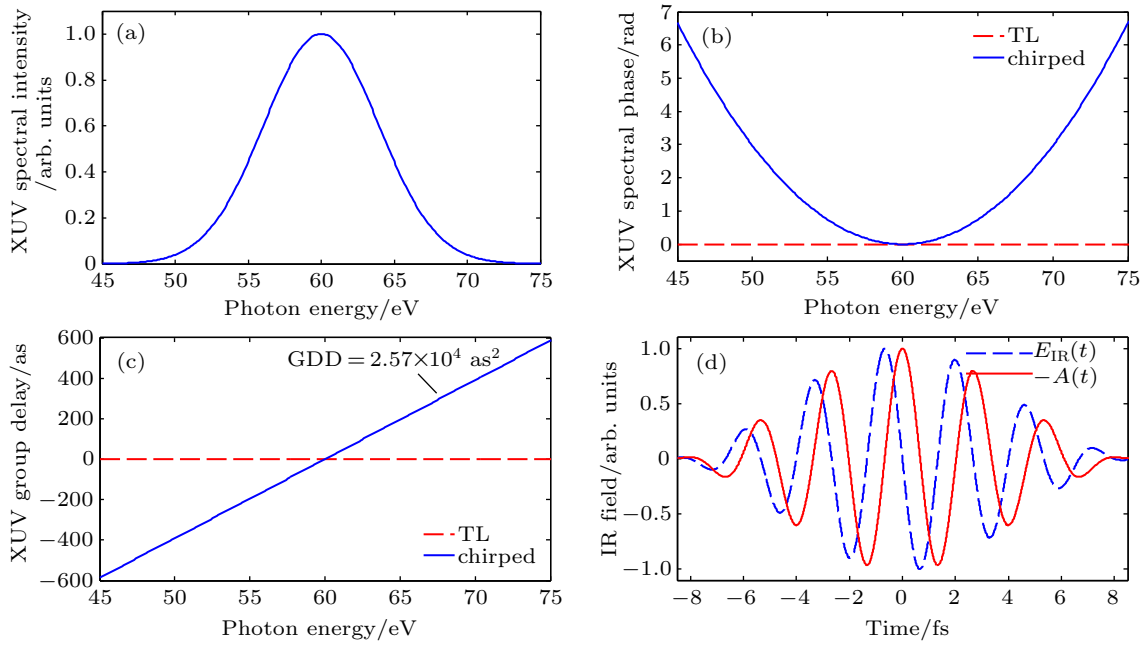


Fig. 1. (a) XUV spectral intensity $U^2(\Omega)$. (b) XUV spectral phase $\Phi(\Omega)$ for a TL pulse (${\rm GDD}^{\rm XUV} = 0$, $\Delta t = 197$ as) and a chirped pulse (${\rm GDD}^{\rm XUV} = 2.57\times10^4$ as^2, $\Delta t = 410$ as). (c) XUV group delay $\tau^{\rm XUV}(\Omega)$. (d) The electric field $E_{\rm IR}(t)$ and vector potential $-A(t)$ of the IR field.

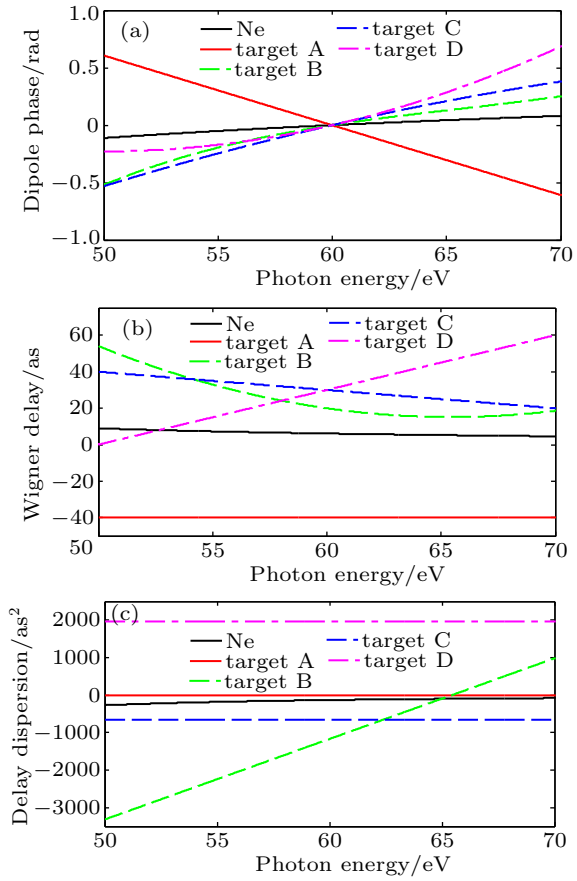


Fig. 2. (a) Dipole phase $\eta(\Omega)$, (b) Wigner delay $\tau^{\rm dip}(\Omega)$, and (c) GDD$^{\rm dip}(\Omega)$ for Ne atom and four artificial targets (A–D).

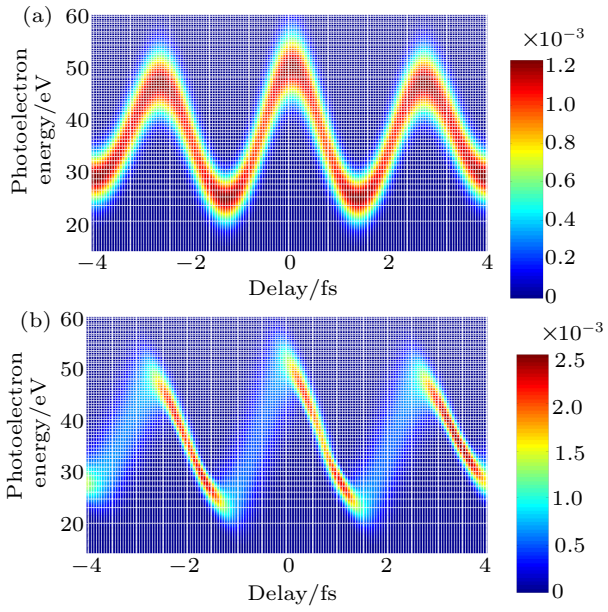


Fig. 3. SFA simulated spectrogram $S(E,t_{\rm d})$ for target A using (a) the 197 as TL XUV and (b) the 410 as chirped XUV.

3.1.2. Streaking spectrograms and their first moments

Figure 3 shows two simulated spectrograms $S(E,t_{\rm d})$ for target A using both the 197 as TL and the 410 as chirped XUV pulses. One can see obvious differences between these two spectrograms. We then calculate their COEs, $\bar{E}(t_{\rm d})$, as shown in Fig. 4(a). A zoom-in plot near $t_{\rm d}=0$ is given in Fig. 4(b). By measuring the peak position of $\bar{E}(t_{\rm d})$ compared with the peak position of $-A(t_{\rm d})$ (at $t_{\rm d}=0$), one can extract the time delay $\tau^{\rm s}$ in Eq. (18). As shown in Fig. 4(b), the extracted $\tau^{\rm s}=-40$ as for the case of TL XUV and $\tau^{\rm s}=-25$ as for the case of 410 as chirped XUV. It is clear how difficult it is to pinpoint the first moment $\bar{E}(t_{\rm d})$ at the level of few to around ten attoseconds accuracy from the calculated spectrograms, not to mention how much error would occur if the experimental data are analyzed. In order to obtain 1 as resolution in time delay, the step size for an experimentalist to adjust the arm of the interferometer should be 0.3 nm. Definitely, to make such precise adjustment is challenging.

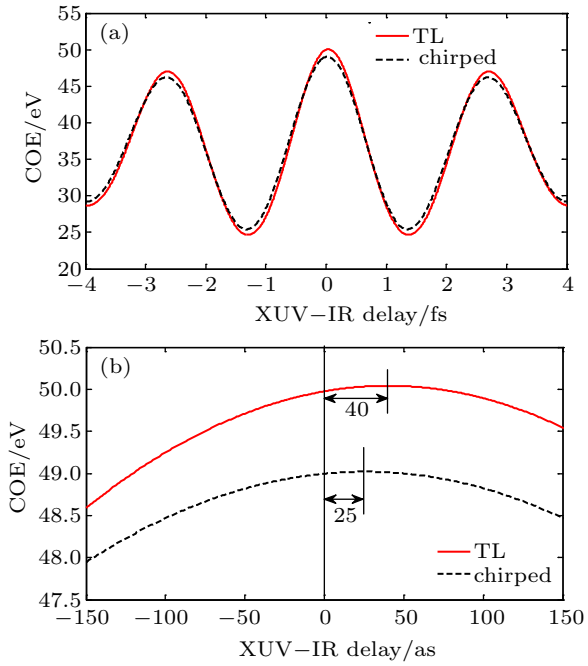


Fig. 4. (a) The COE $\bar{E}(t_{\rm d})$ calculated from the two spectrograms for target A shown in Fig. 3, using both the 197 as TL XUV and the 410 as chirped XUV. (b) A zoom-in plot near $t_{\rm d}=0$ from which one can extract the time delay $\tau^{\rm s}$ in Eq. (18).

3.1.3. Errors of the retrieved time delay due to group delay dispersions

For SFA simulations in this subsection, we expect that $\tau^{\rm s}=\tau_0^{\rm dip}$. However, the retrieved $\tau^{\rm s}$ does not necessarily equal $\tau_0^{\rm dip}$. Table 1 summarizes the extracted time delay $\tau^{\rm s}$ from COE/COM of the spectrograms generated by the 197 as TL XUV, the 410 as chirped XUV, and another two XUV pulses with smaller attochirps (GDD$^{\rm XUV}=\pm1.10\times10^4$ as^2, $\Delta t=250$ as). These numbers are to be compared with the input Wigner delay $\tau_0^{\rm dip}$ at $\Omega_0=60$ eV for different targets. Note that we did two cases for Ne: in one case the dipole amplitude $|d(\Omega)|=$ const, while in another case the actual $|d(\Omega)|$ for Ne was used. As shown in the black solid line in Fig. 5(a), the dipole amplitude for Ne decreases monotonically with the photon energy in the XUV bandwidth. Therefore, the peak photon energy of the wave packet $\tilde{W}(\Omega)$ is 59.5 eV, which differs from the central energy of the XUV spectrum $\Omega_0=60$ eV.

Table 1. Time delay τ^{s} extracted from the COE/COM of the SFA simulated spectrogram using the 197 as TL ($GDD^{XUV}=0$), 250 as chirped ($GDD^{XUV}=\pm 1.10\times 10^{4}$ as^2), and 410 as chirped ($GDD^{XUV}=2.57\times 10^{4}$ as^2) XUV pulses, respectively. These numbers are compared with the input Wigner delay τ_0^{dip} at $\Omega_0=60$ eV. The XUV group delay $\tau_0^{XUV}=0$ at $\Omega_0=60$ eV. The second column gives $GDD^{dip}(\Omega_0)$ for each target. For Ne target, both a constant dipole amplitude and the actual dipole amplitude are used in our simulation.

	$GDD^{dip}(\Omega_0)$	Wigner delay τ_0^{dip}	Extracted delay τ^{s}			
GDD^{XUV}	–	–	0	1.10×10^{4} as^2	2.57×10^{4} as^2	-1.10×10^{4} as^2
Target A	0	−40 as	−40/−40 as	−34/−38 as	−25/−33 as	−46/−43 as
Target B	−1170 as^2	20 as	36/36 as	41/39 as	51/44 as	32/36 as
Target C	−658 as^2	30 as	34/34 as	40/37 as	50/42 as	28/32 as
Target D	1975 as^2	30 as	18/17 as	22/19 as	27/19 as	12/14 as
Ne (constant $\lvert d(\Omega)\rvert$)	−130 as^2	6 as	7/7 as	13/10 as	23/15 as	1/4 as
Ne (actual $\lvert d(\Omega)\rvert$)	−130 as^2	6 as	7/8 as	4/2 as	2/−6 as	11/14 as

From Table 1, we can see that if the TL XUV pulse is used, the time delays extracted from the COE and the COM of the spectrogram agree well with a difference less than 1 as. As $|GDD^{XUV}|$ increases, the difference between COE and COM results also increases. For a positive (negative) GDD^{XUV}, the COM tends to yield a smaller (larger) time delay than the COE. We then take the COE results in the following discussion for example. For target A–D we can conclude that the error between τ^{s} and τ_0^{dip} depends on two factors: GDD^{XUV} and $GDD^{dip}(\Omega)$. The first moment method is accurate only when $GDD^{XUV}=GDD^{dip}(\Omega)=0$, that is, for target A using the TL pulse, $\tau^{s}=\tau_0^{dip}=-40$ as. By looking at the row corresponding to target A in Table 1, we notice that a positive (negative) GDD^{XUV} leads to a positive (negative) error. On the other hand, by looking at the column corresponding to the TL XUV, we can see that a positive (negative) $GDD^{dip}(\Omega_0)$ leads to a negative (positive) error. For the cases that both GDD^{XUV} and GDD^{dip} are non-zero, both GDDs contribute to the error of the extracted time delay. However, GDD^{XUV} and GDD^{dip} affect the extracted time delay in different ways so that the error of the first moment method cannot be attributed to a total delay dispersion $GDD^{XUV}+GDD^{dip}$.

For Ne target using a constant $|d(\Omega)|$, since $GDD^{dip}(\Omega_0)=-130$ as^2 is quite small, the results are similar to the case of target A. The extracted time delay using the TL pulse $\tau^{s}=7$ as is very close to the Wigner delay $\tau_0^{dip}=6$ as. On the other hand, if we use the actual $|d(\Omega)|$ of Ne, the peak energy of the wave packet shifts by −0.5 eV from $\Omega_0=60$ eV. Such an energy shift has negligible effects on τ^{dip} and GDD^{dip}, but has a considerable effect on τ^{XUV} if the XUV has attochirp. We can estimate from $\tau^{XUV}(\Omega)=GDD^{XUV}(\Omega-\Omega_0)$ that $\tau^{XUV}=-20$ as for $GDD^{XUV}=2.57\times 10^{4}$ as^2, and $\tau^{XUV}=\mp 9$ as for $GDD^{XUV}=\pm 1.10\times 10^{4}$ as^2. From the last two rows of Table 1, we can observe the contribution from the non-zero τ^{XUV} to the extracted τ^{s} for chirped XUV pulses. The estimated numbers in general agree with the numbers obtained by comparing the two rows in Table 1.

3.2. Time delays extracted from TDSE simulations

3.2.1. Simulation parameters

In this subsection we take into account the Coulomb–laser coupling by simulating the Ne and Ar spectrogram via solving TDSE. In the TDSE computation, the one-electron model potential[55] and the discrete-variable-representation basis set[56] are used. Three transform-limited XUV pulses were used in the TDSE simulation with the central photon energy $\Omega_0=30$ eV, 35 eV, and 40 eV, respectively. These XUV pulses have a bandwidth $\Delta\Omega=8$ eV and thus a FWHM duration $\Delta t=228$ as. $\tau^{XUV}(\Omega)=0$, and $GDD^{XUV}(\Omega)=0$. The IR field is 800 nm in wavelength, 4.4 fs in FWHM duration, and 5×10^{12} W/cm^2 in peak intensity. The one-electron model potential[55] is used to calculate the single-photon transition dipole for Ne and Ar. Figure 5(a) shows the dipole amplitude $|d(\Omega)|$ as a function of photon energy Ω, from which the Cooper minimum of Ar[57] can be observed at $\Omega=42$ eV. The dipole phase $\eta(\Omega)$ is plotted in Fig. 5(b). Figures 5(c) and 5(d) show the input Wigner delay $\tau^{dip}(\Omega)$, the CLC delay $\tau^{CLC}(\Omega)$, and Wigner+CLC delay $\tau^{dip}(\Omega)+\tau^{CLC}(\Omega)$ for Ne and Ar, respectively. The corresponding delay dispersions are plotted in Fig. 6.

3.2.2. Comparison between the retrieved time delay with the input

From the COE of the computed TDSE spectrograms, we extract the streaking time delays τ^{s} at three central photon energies of the XUV pulses, $\Omega_0=30$ eV, 35 eV, and 40 eV. Due to the non-constant dipole amplitude $|d(\Omega)|$, the extracted τ^{s} should be compared with the input τ^{dip} or $\tau^{dip}+\tau^{CLC}$ at the peak energy of the wave packet instead of Ω_0. The numbers of input and extracted time delays are compared in Table 2. The extracted streaking delays are also shown by "+" markers in Figs. 5(c) and 5(d).

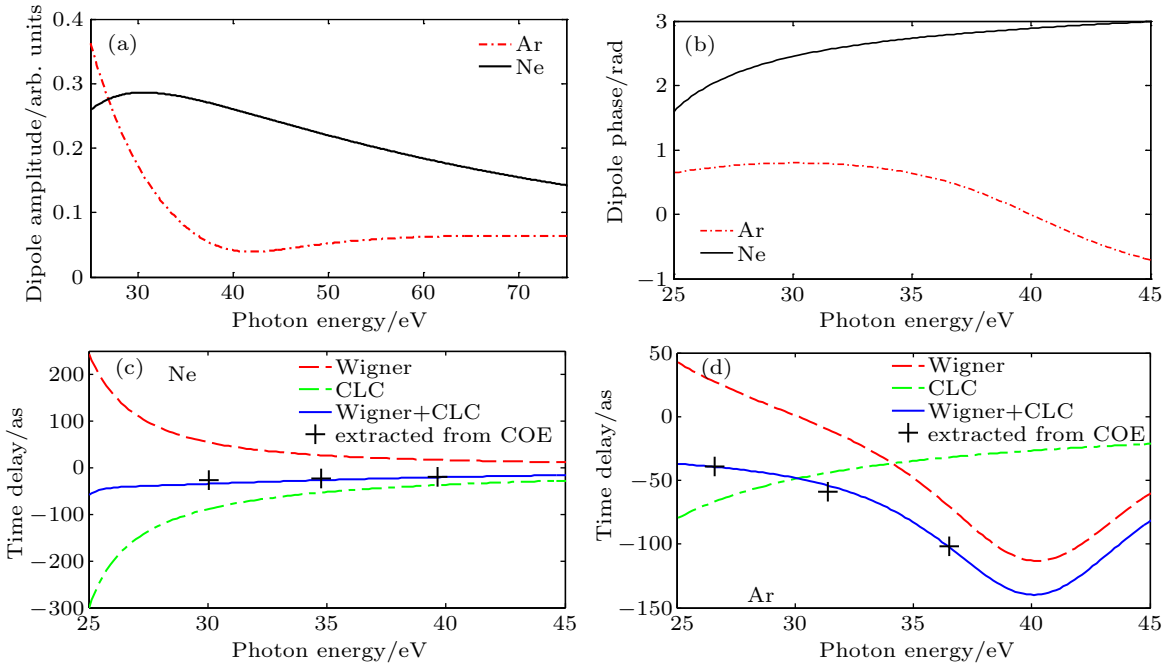


Fig. 5. (a) Dipole amplitude $|d(\Omega)|$ and (b) dipole phase $\eta(\Omega)$ for Ne and Ar targets, calculated using one-electron model potential.[55] From the dipole phase one can obtain the Wigner delay $\tau^{\rm dip}(\Omega) = {\rm d}\eta(\Omega)/{\rm d}\Omega$, as shown in the dashed lines in (c) for Ne and (d) for Ar. After including the CLC correction[37] $\tau^{\rm CLC}(\Omega)$ as plotted in the dot-dashed lines, the Wigner+CLC delay $\tau^{\rm dip}(\Omega)+\tau^{\rm CLC}(\Omega)$ can be obtained as in the solid lines. The markers "+" are the extracted time delays $\tau^{\rm s}$ from the COE of the TDSE spectrograms.

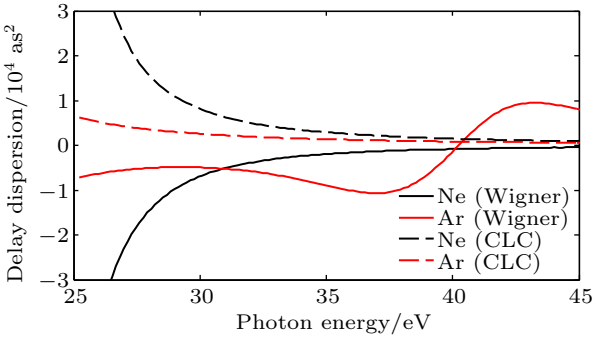


Fig. 6. The group delay dispersion corresponding to the Wigner part ${\rm GDD}^{\rm dip}(\Omega) = {\rm d}\tau^{\rm dip}(\Omega)/{\rm d}\Omega$ and to the CLC part ${\rm GDD}^{\rm CLC}(\Omega) = {\rm d}\tau^{\rm CLC}(\Omega)/{\rm d}\Omega$, for both Ne and Ar.

Table 2. Comparison between the input Wigner delay $\tau^{\rm dip}$, Wigner+CLC delay $\tau^{\rm dip}+\tau^{\rm CLC}$ at the peak photon energy of the electron wave packet and the extracted time delay $\tau^{\rm s}$ from the COE/COM of the TDSE simulated spectrogram, using three TL XUV pulses with central photon energies $\Omega_0 = 30$ eV, 35 eV, and 40 eV for both Ne and Ar. The XUV group delay $\tau^{\rm XUV} = 0$.

	$\Omega_0 = 30$ eV	$\Omega_0 = 35$ eV	$\Omega_0 = 40$ eV
peak energy (Ne)	30.06 eV	34.77 eV	39.65 eV
$\tau^{\rm dip}$ (Ne)	53 as	27 as	17 as
$\tau^{\rm dip}+\tau^{\rm CLC}$ (Ne)	−35 as	−27 as	−21 as
$\tau^{\rm s}$ (Ne)	−26/−28 as	−23/−24 as	−20/−20 as
peak position (Ar)	26.59 eV	31.39 eV	36.53 eV
$\tau^{\rm dip}$ (Ar)	27 as	−10 as	−71 as
$\tau^{\rm dip}+\tau^{\rm CLC}$ (Ar)	−40 as	−54 as	−103 as
$\tau^{\rm s}$ (Ar)	−39/−38 as	−59/−58 as	−102/−101 as

Table 2 shows that when TL pulses are used, the time delays from COE and COM are quite close to each other. Their difference is less than 2 as. Generally speaking, the extracted time delay agrees with the input Wigner+CLC delay for both Ne and Ar. For Ne target, the errors of the COE method are 9 as, 4 as, and 1 as, respectively, while for Ar target the errors are 1 as, −5 as, and 1 as, respectively. Since $\tau^{\rm XUV}(\Omega) = 0$, ${\rm GDD}^{\rm XUV}(\Omega) = 0$, the error depends on ${\rm GDD}^{\rm dip}(\Omega)$ and ${\rm GDD}^{\rm CLC}(\Omega) = {\rm d}\tau^{\rm CLC}(\Omega)/{\rm d}\Omega$. From Fig. 6, we can see that for both Ne and Ar, the positive ${\rm GDD}^{\rm CLC}(\Omega)$ can compensate the negative ${\rm GDD}^{\rm dip}(\Omega)$ in the vicinity of the peak photon energy of the wave packet, which helps to reduce the error between the extracted and the input time delay. This example shows that after considering the shift in the peak energy of the photoelectron wave packet with respect to the central energy of the XUV field, and considering the effect of Coulomb–laser coupling, it is possible to extract photoionization time delays from TDSE simulated streaking spectrograms.

4. Conclusions

We have simulated streaking spectrograms based on the SFA model and TDSE calculation using various targets and XUV pulses. From the first moment of the spectrogram, we have extracted a photoionization time delay and compared it with the input Wigner delay (or Wigner+CLC delay for low-energy electrons) at the peak photon energy of the electron wave packet. The main conclusion is that the first moment method is accurate only when the GDDs corresponding to both the XUV spectral phase and the transition dipole phase (including the CLC term for low-energy electrons) are small. In this situation, the wave packet can be characterized by a single group delay and behaves as a classical particle in the

dressing IR field. The energy or momentum modulation in the spectrogram can then be interpreted classically which serves as the prerequisite of the first moment method. Otherwise, if large GDD in either the XUV part or the transition dipole part is present, the propagation of the wave packet in the laser field is complicated which is a consequence of the wave property of the photoelectron. Different energy components of the wave packet behave differently in the streaking field and therefore a total group delay is not reasonable any more to interpret the spectrogram. We have demonstrated that the first moment method is not reliable in the case of large GDDs. In a real experiment, the generated XUV pulse often has some attochirp, and the IR field is not exactly known; therefore, to achieve the time delay from the first moment with an accuracy of a few to few tens of attoseconds is challenging.

An electron wave packet, like in optics, can have spectral amplitude and spectral phase. In optics, the derivative of the phase with respect to frequency is called group delay. Likewise, the phase of an electron wave with respect to energy can also be called a group delay. Since the group delay has the unit of time, it has also been called the time delay in the streaking experiment. In particular, a single value of the time delay has often been assigned to a wave packet, taken to be the group delay (the derivative of the phase) at the peak position of the photoelectron spectrum. The fallacy of such a simplification is obvious. An electron wave packet clearly has a spectral distribution, and by definition, the group delay has to be specified over the whole spectral distribution of the wave packet. In optics, a single group delay can represent the whole wave packet only if the pulse is transform-limited. Likewise, a single group delay cannot represent the group delay of the whole electron wave packet unless its group delay is constant over the whole spectral width. The controversy or debate of photoionization time delay would not have been necessary if one has not used a single group delay at a specific energy to represent the group delay of the whole wave packet and if this group delay is not called a time delay which connotate the delayed arrival of a classical electron at the detector, especially when such delays are at the attosecond scale.

References

[1] Paul P M, Toma E S, Breger P, Mullot G, Augé F, Balcou P, Muller H G and Agostini P 2001 *Science* **292** 1689

[2] Hentschel M, Kienberger R, Spielmann C, Reider G A, Milosevic N, Brabec T, Corkum P, Heinzmann U, Drescher M and Krausz F 2001 *Nature* **414** 509

[3] Goulielmakis E, Schultze M, Hofstetter M, Yakovlev V S, Gagnon J, Uiberacker M, Aquila A L, Gullikson E M, Attwood D T, Kienberger R, Krausz F and Kleineberg U 2008 *Science* **320** 1614

[4] Zhao K, Zhang Q, Chini M, Wu Y, Wang X and Chang Z H 2012 *Opt. Lett.* **37** 3891

[5] Guo X L, Zhao S F, Wang G L and Zhou X X 2018 *Chin. Phys. B* **27** 43201

[6] Xu Q Y, Tian Y R, Lu H Z, Zhang J, Xu T T, Zhang H D, Liu X S and Guo J 2018 *Chin. Phys. B* **27** 33202

[7] Pan X F, Zhang J, Ben S, Xu T T and Liu X S 2018 *Chin. Phys. B* **27** 24206

[8] Zhao X, Chen J, Fu P, Liu X, Yan Z C and Wang B 2013 *Phys. Rev. A* **87** 043411

[9] Guo J, Ge X L, Zhong H Y, Zhao X, Zhang M, Jiang Y and Liu X S 2014 *Phys. Rev. A.* **90** 053410

[10] Klünder K J, Dahlström M, Gisselbrecht M, Fordell T, Swoboda M, Guénot D, Johnsson P, Caillat J, Mauritsson J, Maquet A, Taïeb R and L'Huillier A 2011 *Phys. Rev. Lett.* **106** 143002

[11] Xia C L, Ge X L, Zhao X, Guo J and Liu X S 2012 *Phys. Rev. A* **85** 053424

[12] Zhao X, Yang Y J, Liu X S and Wang B 2014 *Chin. Phys. Lett.* **31** 043202

[13] Palatchi C, Dahlström J M, Kheifets A S, Ivanov I A, Canaday D M, Agostini P and DiMauro L F 2014 *J. Phys. B: At. Mol. Opt. Phys.* **47** 245003

[14] Zhai Z, Peng D, Zhao X, Guo F, Yang Y, Fu P, Chen J, Yan Z C and Wang B 2012 *Phys. Rev. A* **86** 043432

[15] Gruson V, Barreau L, Jiménez-Galan Á, Risoud F, Caillat J, Maquet A, Carré B, Lepetit F, Hergott J F, Ruchon T, Argenti L, Taïeb R, Martin F and Saliéres P 2016 *Science* **354** 734

[16] Schultze M, Fieß M, Karpowicz N, *et al.* 2010 *Science* **328** 1658

[17] Sabbar M, Heuser S, Boge R, Lucchini M, Carette T, Lindroth E, Gallmann L, Cirelli C and Keller U 2015 *Phys. Rev. Lett.* **115** 133001

[18] Ossiander M, Siegrist F, Shirvanyan V, Pazourek R, Sommer A, Latka T, Guggenmos A, Nagele S, Feist J, Burgdörfer J, Kienberger R and Schultze M 2017 *Nat. Phys.* **13** 280

[19] Uiberacker M, Uphues T, Schultze M, Verhoef A J, Yakovlev V, Kling M F, Rauschenberger J, Kabachnik N M, Schröder H, Lezius M, Kompa K L, Muller H G, Vrakking M J J, Hendel S, Kleineberg U, Heinzmann U, Drescher M and Krausz F 2007 *Nature* **446** 627

[20] Tzallas P, Skantzakis E, Nikolopoulos L A A, Tsakiris G D and Charalambidis D 2011 *Nat. Phys.* **7** 781

[21] Månsson E P, Guénot D, Arnold C L, Kroon D, Kasper S, Dahlström J M, Lindroth E, Kheifets A S, L'Huillier A, Sorensen S L and Gisselbrecht M 2014 *Nat. Phys.* **10** 207

[22] Caillat J, Maquet A, Haessler S, Fabre B, Ruchon T, Salières P, Mairesse Y and Taïeb R 2011 *Phys. Rev. Lett.* **106** 093002

[23] Kelkensberg F, Siu W, Pérez-Torres J F, Morales F, Gademann G, Rouzée A, Johnsson P, Lucchini M, Calegari F, Sanz-Vicario J L, Martin F and Vrakking M J J 2011 *Phys. Rev. Lett.* **107** 043002

[24] Sansone G, Kelkensberg F, Pérez-Torres J F, *et al.* 2010 *Nature* **465** 763

[25] Calegari F, Ayuso D, Trabattoni A, Belshaw L, De Camillis S, Anumula S, Frassetto F, Poletto L, Palacios A, Decleva P, Greenwood J B, Martin F and Nisoli M 2014 *Science* **346** 336

[26] Trabattoni A, Klinker M, González-Vázquez J, Liu C, Sansone G, Linguerri R, Hochlaf M, Klei J, Vrakking M J J, Martin F, Nisoli M and Calegari F 2015 *Phys. Rev. X* **5** 041053

[27] Cavalieri A L, Müller N, Uphues T, Yakovlev V S, Baltuska A, Horvath B, Schmidt B, Blümel L, Holzwarth R, Hendel S, Drescher M, Kleineberg U, Echenique P M, Kienberger R, Krausz F and Heinzmann U 2007 *Nature* **449** 1029

[28] Neppl S, Ernstorfer R, Bothschafter E M, Cavalieri A L, Menzel D, Barth J V, Krausz F, Kienberger R and Feulner P 2012 *Phys. Rev. Lett.* **109** 087401

[29] Neppl S, Ernstorfer R, Cavalieri A L, Lemell C, Wachter G, Magerl E, Bothschafter E M, Jobst M, Hofstetter M, Kleineberg U, Barth J V, Menzel D, Burgdörfer J, Feulner P, Krausz F and Kienberger R 2015 *Nature* **517** 342

[30] Lemell C, Neppl S, Wachter G, Tőkési K, Ernstorfer R, Feulner P, Kienberger R and Burgdörfer J 2015 *Phys. Rev. B* **91** 241101

[31] Locher R, Castiglioni L, Lucchini M, Greif M, Gallmann L, Osterwalder J, Hengsberger M and Keller U 2015 *Optica* **2** 405

[32] Tao Z, Chen C, Szilvási T, Keller M, Mavrikakis M, Kapteyn H and Murnane M 2016 *Science* **353** 62

[33] Itatani J, Quéré F, Yudin G L, Ivanov M Y, Krausz F and Corkum P B 2002 *Phys. Rev. Lett.* **88** 173903

[34] Muller H G 2002 *Appl. Phys. B* **74** S17

[35] Mairesse Y and Quéré F 2005 *Phys. Rev. A* **71** 011401

[36] Maquet A, Caillat J and Taïeb R 2014 *J. Phys. B: At. Mol. Opt. Phys.* **47** 204004

[37] Pazourek R, Nagele S and Burgdörfer J 2015 *Rev. Mod. Phys.* **87** 765

[38] Kheifets A S and Ivanov I A 2010 *Phys. Rev. Lett.* **105** 233002

[39] Moore L R, Lysaght M A, Parker J S, van der Hart H W and Taylor K T 2011 *Phys. Rev. A* **84** 061404
[40] Dahlström J M, Carette T and Lindroth E 2012 *Phys. Rev. A* **86** 061402(R)
[41] Nagele S, Pazourek R, Feist J and Burgdörfer J 2012 *Phys. Rev. A* **85** 033401
[42] Pazourek R, Feist J, Nagele S and Burgdörfer J 2012 *Phys. Rev. Lett.* **108** 163001
[43] Feist J, Zatsarinny O, Nagele S, Pazourek R, Burgdörfer J, Guan X, Bartschat K and Schneider B I 2014 *Phys. Rev. A* **89** 033417
[44] Kazansky A K and Echenique P M 2009 *Phys. Rev. Lett.* **102** 177401
[45] Borisov A G, Sánchez-Portal D, Kazansky A K and Echenique P M 2013 *Phys. Rev. B* **87** 121110(R)
[46] Zhang C H and Thumm U 2011 *Phys. Rev. A* **84** 033401
[47] Liao Q and Thumm U 2014 *Phys. Rev. Lett.* **112** 023602
[48] Calegari F, Sansone G, Stagira S, Vozzi C and Nisoli M 2016 *J. Phys. B: At. Mol. Opt. Phys.* **49** 062001
[49] Wigner E P 1955 *Phys. Rev.* **98** 145
[50] Smith F T 1960 *Phys. Rev.* **118** 349
[51] Zhao X, Wei H, Wu Y and Lin C D 2017 *Phys. Rev. A* **95** 043407
[52] Kitzler M, Milosevic N, Scrinzi A, Krausz F and Brabec T 2002 *Phys. Rev. Lett.* **88** 173904
[53] Yakovlev V S, Gagnon J, Karpowicz N and Krausz F 2010 *Phys. Rev. Lett.* **105** 073001
[54] Zhao X, Wei H, Wei C and Lin C D 2017 *J. Opt.* **19** 114009
[55] Tong X M and Lin C D 2005 *J. Phys. B: At. Mol. Opt. Phys.* **38** 2593
[56] Morishita T, Chen Z, Watanabe S and Lin C D 2007 *Phys. Rev. A* **75** 023407
[57] Cooper J W 1962 *Phys. Rev.* **128** 681